Environment International 174 (2023) 107904

Contents lists available at ScienceDirect

Environment International

journal homepage: www.elsevier.com/locate/envint

Full length article

Buffering effect of global vegetation on the air-land exchange of mercury: Insights from a novel terrestrial mercury model based on CESM2-CLM5

Tengfei Yuan [a], Peng Zhang [a], Zhengcheng Song [a], Shaojian Huang [a], Xun Wang [c], Yanxu Zhang [a,b,*]

[a] School of Atmospheric Sciences, Nanjing University, Nanjing, Jiangsu 210023, China
[b] Frontiers Science Center for Critical Earth Material Cycling, Nanjing University, Nanjing 210023, China
[c] State Key Laboratory of Environmental Geochemistry, Institute of Geochemistry, Chinese Academy of Sciences, Guiyang 550081, China

ARTICLE INFO

Keywords:
Mercury budget
CLM5-Hg
Hg(0) vegetation uptake
litter Hg concentration
Lagging effect
Physiology
Sequestration

ABSTRACT

The vegetation uptake of atmospheric elemental mercury [Hg(0)] and its subsequent littering are critical processes of the terrestrial Hg cycles. There is a large uncertainty in the estimated global fluxes of these processes due to the knowledge gap in the underlying mechanisms and their relationship with environmental factors. Here, we develop a new global model based on the Community Land Model Version 5 (CLM5-Hg) as an independent component of the Community Earth System Model 2 (CESM2). We explore the global pattern of gaseous elemental Hg [Hg(0)] uptake by vegetation and the spatial distribution of litter Hg concentration constrained by observed datasets as well as its driving mechanism. The annual vegetation uptake of Hg(0) is estimated as 3132 Mg yr^{-1}, which is considerably higher than previous global models. The scheme of dynamic plant growth including stomatal activities substantially improves the estimation for global terrestrial distribution of Hg, compared to the leaf area index (LAI) based scheme that is often used by previous models. We find the global distribution of litter Hg concentrations driven by vegetation uptake of atmospheric Hg(0), which are simulated to be higher in East Asia (87 ng/g) than in the Amazon region (63 ng/g). Meanwhile, as a significant source for litter Hg, the formation of structural litter (cellulose litter + lignin litter) results in a lagging effect between Hg(0) deposition and litter Hg concentration, implying the buffering effect of vegetation on the air-land exchange of Hg. This work highlights the importance of vegetation physiology and environmental factors in understanding the vegetation sequestration of atmospheric Hg globally, and calls for greater efforts to protect forests and afforestation.

1. Introduction

Mercury is a neurotoxin that can harm human health (Beckers and Rinklebe, 2017). It is also an environmental pollutant that cycles globally between the atmosphere, land, oceans, and ecosystems within (Obrist et al., 2018). The terrestrial ecosystem is an important part of the global Hg cycle due to the large mass of Hg in soils and the active bi-directional exchange of Hg between the atmosphere and the heterogeneous land surfaces (Agnan et al., 2016). The uptake of gaseous elemental Hg (Hg0) by vegetation is a crucial process via which atmospheric Hg enters terrestrial ecosystems (Gustin et al., 2008; Obrist et al., 2017). The foliar Hg concentrations are positively correlated with atmospheric Hg levels (Fay and Gustin, 2007; Millhollen et al., 2006) and the vegetation was found to determine the partition of Hg deposition to the ocean and land globally (Zhou et al., 2021). The seasonal variations of atmospheric Hg concentrations are also related to foliage photosynthetic activity and subsequent atmospheric CO_2 concentrations as a result of vegetation uptake (Fu et al., 2019; Jiskra et al., 2018; St. Louis et al., 2019).

Large uncertainties (1000–1400 Mg) exist in our estimate of global Hg(0) vegetation uptake (Horowitz et al., 2017; Outridge et al., 2018; Zhou et al., 2021,2016), most of which are derived from an upscaling of limited observations. The uncertainties are caused by the following reasons: i. the observational data is limited to remote and vegetated regions, especially in the tropical/subtropical forest regions that possess the large potential to uptake Hg (Yuan et al., 2019b), but ignores vegetated regions with higher anthropogenic emissions, i.e. the mid-latitudes; ii. the estimate of global Hg deposition by litterfall does not

* Corresponding author at: School of Atmospheric Sciences, Nanjing University, Nanjing, Jiangsu 210023, China.
E-mail address: zhangyx@nju.edu.cn (Y. Zhang).

https://doi.org/10.1016/j.envint.2023.107904
Received 9 November 2022; Received in revised form 4 March 2023; Accepted 26 March 2023
Available online 31 March 2023

account for woody tissues, underlying soils, and nonvascular plants (Obrist et al., 2018). A part of atmospheric Hg will remain in the plant and be distributed to woody tissues by phloem and xylem transport (Liu et al., 2021; Obrist et al., 2018; Wang et al., 2021; Zhou and Obrist, 2021). A significant proportion of Hg is assimilated by lichens, mosses, and woody tissues including roots (Zhou and Obrist, 2021); iii. the lack of consideration for multiple vegetation/plant function types that have different Hg(0) uptake efficacies, for instance, the mangrove and evergreen broadleaf usually have a higher Hg concentration in foliage than other tree species (Wang et al., 2021).

The Hg(0) taken by the leaf also undergoes various chemical reactions such as oxidation, reduction, and complexation, resulting in retention within the foliage, which is subsequently transferred to soil as litterfall when the leaf abscises and plants die off (Liu et al., 2021; Obrist et al., 2018). Thus, litterfall Hg plays a key role in the ecosystem process of the global Hg cycle (Wang et al., 2016a; Zhou et al., 2018). A series of local studies have shown that litterfall Hg deposition is the main Hg input for forest floor Hg (Jiskra et al., 2015; Luo et al., 2022; Pokharel and Obrist, 2011; Risch et al., 2012; Wang et al., 2017), however, the mechanisms for the global distribution of litter Hg concentration are not well understood. The litterfall biomass was often considered the dominant factor (Zhou et al., 2018,2016), but the influence of atmospheric Hg concentration was largely neglected. Indeed, some sites in East Asia are found to have higher litterfall Hg concentrations than the Amazon area which has the largest aboveground litterfall biomass (Li et al., 2019). For another, wildfire Hg emissions are influenced by a variety of environmental and anthropogenic factors, including climate conditions, geography, the type of vegetation, the extent and type of human activity, as well as the Hg content in different vegetation tissues (De Simone et al., 2015; Kumar et al., 2018).

Process-based global models have been developed to study the terrestrial Hg cycles (Schaefer et al., 2020; Smith-Downey et al., 2010). However, these models didn't consider critical processes such as vegetation uptake, soil Hg leaching, and wildfires. Moreover, these models often merely rely on the leaf area index (LAI) to calculate the vegetation uptake of Hg(0) but ignore the variability of stomatal uptake, which is regarded as the dominant pathway of Hg incorporated into foliar. These estimations could thus bear massive bias compared with the observations. The stomatal conductance is a key indicator of plant Hg uptake (Laacouri et al., 2013; Rutter et al., 2011a, 2011b; Stamenkovic and Gustin, 2009), and the related bidirectional air-surface exchange of Hg (0) has been incorporated by previous modeling studies (Bash, 2010; Khan et al., 2019; Wang et al., 2016c; Zhang et al., 2016b). Here, we develop a new mechanistic terrestrial ecosystem Hg model based on Community Land Model v5 (CLM5-Hg) within the Community Earth System Model v2 (CESM2). CLM5 is one of the most comprehensive land surface models, which has more ecological process fidelity than previous models, such as stomatal physiology and dynamic land units based on prognostic global vegetation state (Lawrence et al., 2019). This model thus could help us to better understand the Hg cycles in the terrestrial ecosystems covering different plant functional types (PFT). Here, we add Hg species as new tracers into the CLM5. The related process in terrestrial Hg cycle, such as the stomatal regulation, soil emission, soil leaching, chemical transformation of leaf and underground soil reservoirs, and wildfires are also included (Fig. 1). We explore the global pattern of Hg(0) uptake by vegetation based on various PFT, which is compared with the LAI method. We also assess the litter Hg concentration distributions constrained by observed datasets and explore the mechanism for driving the global spatial distribution of litter Hg.

2. Methodology

2.1. Model overview

We develop a mechanical simulation of the Hg cycle in the terrestrial ecosystems that are coupled with the bio-geophysical and biogeochemical process within the CLM5 (Fig. 1), which is the default land component for the Community Earth System Model Version 2 (CESM2) including comprehensive carbon and nitrogen cycles within the aboveground and belowground process. The terrestrial component is closely coupled with the atmosphere and the state of vegetation (leaf area index [LAI], steam area index [SAI], canopy top and bottom heights, etc.) is prognostically calculated. The CLM phenology model comprises multiple algorithms that regulate the movement of stored carbon and nitrogen out of storage pools for the display of new growth and into litter pools for losses of displayed growth. These algorithms represent different phenological types, each associated with a particular plant functional type (PFT) (Lawrence et al., 2019). The model adopts a

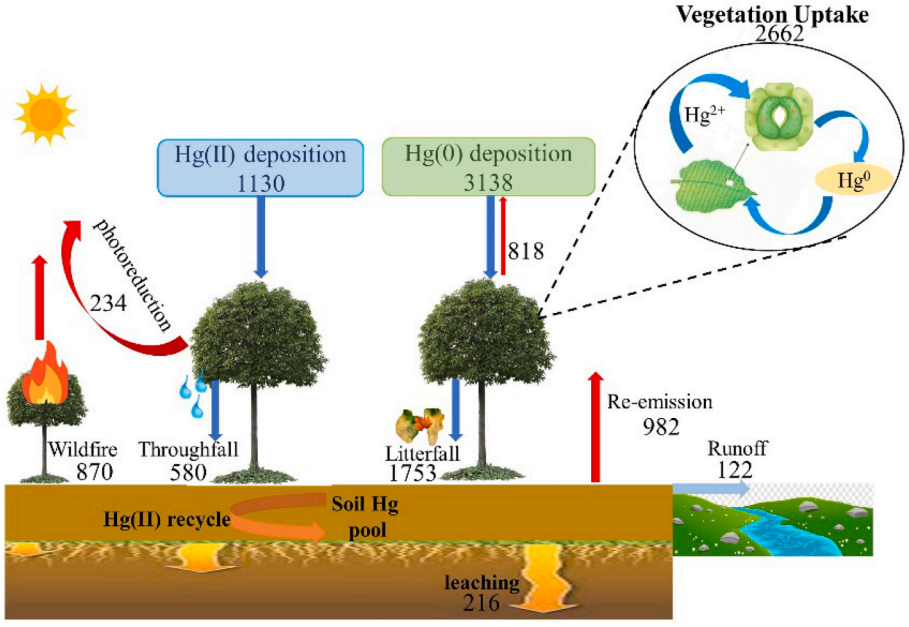

Fig. 1. Terrestrial Hg budget simulated by CLM5-Hg. Numbers represent the Hg flux among pools as well as the emission and deposition fluxes (units are in Mg Hg per year).

demographically structured approach for the dynamic of vegetation, which is the "Functionally Assembled Terrestrial Ecosystem Simulator" in CLM5. The submodule contains vegetation competition and co-existence. It enables a biosphere representation that accounts for the division of the land surface into successional stages, as well as competition for light between height-structured cohorts of representative trees of various plant functional types. The fire emissions are coupled to the atmosphere and the soil module of CLM5 also has a relatively high vertical resolution with 25 layers extending down to 8.50 m (Lawrence et al., 2019).

We use the offline model of CLM5 (0.90° latitude × 1.25° longitude) with coupled biogeochemical cycles (BGC), which is run for 200 years to get a steady state. The model is then run for four years (2011–2014) with the last year used for analysis. The CLM5-Hg model takes the atmospheric Hg(0) concentrations and the dry and wet deposition fluxes of Hg(II) simulated by the CAM6-Chem model as the upper boundary conditions (Zhang and Zhang, 2022) (Fig. S1). The Hg(II) deposition is absorbed on the leaf surface and it landed on the soil surface via throughfall (Smith-Downey et al., 2010; Zhang et al., 2020). The meteorological forcing data of CLM5 is from the Global Soil Wetness Project dataset (GSWP3), which is a 3-hourly 0.5° global forcing product based on 20th Century Reanalysis version 2 (Lawrence et al., 2016).

2.2. Vegetation uptake of Hg(0)

CLM5 adopts a nested sub-gridded hierarchy approach to represent the heterogeneity of land surfaces: unit -> column -> patch. Each model grid cell includes multiple land units (glacier, lake, urban, vegetated, and crop), and each column has various patches, which can take one of the 15 PFT, 4 crop functional types (CFT), and bare ground. We merge four CFTs into one ("Crop") for simplicity. These function types differ in leaf and stem properties that determine the reflectivity, transmittance, and absorption of solar radiation (Table S1); aerodynamic parameters that control resistance to heat, moisture, and momentum transfer; and photosynthetic parameters that determine photosynthesis, stomatal resistance, and transpiration (Lawrence et al., 2019).

The atmospheric Hg(0) uptake by vegetation is calculated as a dry deposition flux (Khan et al., 2019):

$$F_d(z) = V_d C_{(z)} \quad (1)$$

where $F_d(Z)$ represents the Hg(0) dry deposition flux at the height z, $C_{(z)}$ is the atmospheric Hg(0) concentrations from the CAM-Chem model (Zhang and Zhang, 2022), and v_d is the dry deposition velocity calculated following the Wesely scheme (Wesely, 1989):

$$V_d = \frac{1}{R_a + R_b + R_c} \quad (2)$$

where R_a is the aerodynamic resistance between a specific height and the surface, R_b is the quasi-laminar sublayer resistance, and R_c is the bulk surface resistance. R_c is mainly determined by the stomatal resistance (R_s), which is calculated by Medlyn stomatal conductance model (Medlyn et al., 2012) The leaf stomatal resistance is:

$$\frac{1}{r_s} = g0 + 1.6\left(1 + \frac{g1}{\sqrt{D}}\right)\frac{A_n}{C_s/P_{atm}} \quad (3)$$

where g0 is the minimum stomatal conductance, A_n is leaf net photosynthesis, C_s is the CO_2 partial pressure at the leaf surface, P_{atm} is the atmospheric pressure, and D is the vapor pressure deficit at the leaf surface. g_1 is a parameter that depends on the plant functional type (Table S2) following the CABLE model (De Kauwe et al., 2015). r_s is corrected by partitioning sunlit leaf stomatal resistance and shaded leaf stomatal resistance and the condition of snow cover (Lawrence et al., 2019):

$$R_s = \left(\frac{f_{sun} \times \text{elai}}{r_s^{sun}} - \frac{f_{sun} \times elai}{r_s^{sha}}\right)^{\wedge -1} \quad (4)$$

where R_s represents the adjusted stomatal resistance, f_{sun} is sunlit fraction of canopy, elai represents one-sided LAI buried by snow, rsun s is sunlit leaf stomatal resistance, rsha s is shaded leaf stomatal resistance.

2.3. Vegetation and soil Hg pools

The Hg cycle is influenced by the cycle of carbon (C) and is simulated within the C cycling framework (Schaefer et al., 2020; Smith-Downey et al., 2010). CLM5 considers both the above- and below-ground processes, including 18 plant pools consisting of six tissues, six accompanied storage pools, and six transfer pools. Each soil layer is comprised of seven pools for litter and soil organic matter (SOM): metabolic litter (LITR1), cellulose litter (LITR2), lignin litter (LITR3), coarse woody debris (CWD), fast SOM (SOM1), slow SOM (SOM2), and passive SOM (SOM3). The CLM5-Hg considers a corresponding Hg pool for each C pool. C and Hg are transferred from one pool to another, and the flow of C and Hg from one pool to the other reflects the life cycle of organic matter. We use the Hg concentration dataset in surface soil as the initial soil Hg (Wang et al., 2019), where Hg emissions to the atmosphere are based on the decomposition of soil carbon. Some of the C/Hg pools are also released to the atmosphere by CO_2 respiration and Hg(0) emission to the atmosphere (Fig. S2).

The dynamics of vegetation are controlled by its phenology which determines the leaf onset and offset dates through air temperature and soil water conditions. During the offset period, the leaf and fine root die to form litterfall and the LAI drops quickly. The occurrence of fire events is triggered by the amount of litter and soil moisture, while the C and Hg in plant pools are released to the atmosphere or transferred to litter pools determined by their tissue and burning areas. The atmospheric Hg is assimilated by the leaf and transferred to litterfall when plants are at offset period, which is subsequently bound to SOM with considerably high affinity and is shielded from reduction until the organic matter is respired by microbe (Lawrence et al., 2019; Schaefer et al., 2020; Smith-Downey et al., 2010). Moreover, Hg(0) is released into the atmosphere by photoreduction (Saiz-Lopez et al., 2022; Yuan et al., 2019a), leaching of soil (Miretzky et al., 2005; Schaefer et al., 2020; Sun et al., 2019) and wildfire (Kohlenberg et al., 2018) (Fig. 1).

2.4. Observational dataset

The observed litterfall Hg concentration is obtained from the global Hg concentration of plant tissues (Zhou et al., 2021), which summarizes published data between 1976 and 2020, including 2490 individual data points from 230 scientific studies. Data were not weighted by sampling years, since no clear temporal trends in litter Hg concentration were observed among the 40 years (Zhou et al., 2021). Furthermore, although atmospheric mercury concentrations have changed markedly over the last decade, litter and soil mercury concentrations have changed more slowly, as they need longer-term accumulation and transformation before notable changes (Gworek et al., 2020). These data are from 416 different measurement sites across the world covering a variety of vegetation types containing deciduous trees, coniferous trees, evergreen broadleaved trees, grasslands, and fewer wetlands. The 322 records of litter Hg concentration within the dataset are used for model evaluation. Feinberg et al. (2022). This database contains 79 publications with measurements ranged from 1987 to 2020 (Feinberg et al., 2022).

3. Result and discussion

3.1. Terrestrial Hg budget

Fig. 1 shows the budget of the terrestrial Hg cycles from the CLM5-Hg

simulation, including the process of Hg(0) and Hg(II) within the terrestrial ecosystem. The global total Hg(II) deposition is 1130 Mg yr^{-1} to land (Zhang and Zhang, 2022). The global Hg(0) deposition is simulated as 3132 Mg yr^{-1}, more than double of Hg(II) deposition. The foliar Hg(0) re-emission is simulated as 470 Mg yr^{-1}, resulting in a net Hg(0) uptake of 2667 Mg yr^{-1}. The Hg(0) deposition is dominated by vegetation uptake, and a portion of Hg (580 Mg yr^{-1}) deposited on leaf surfaces is washed off with throughfall. After a series of chemical reactions such as oxidation, reduction, and complexation (Fig. 1), the Hg within foliage subsequently enters the surface of the land in the form of litterfall. The global total Hg litterfall flux is estimated as 1753 Mg yr^{-1}, significantly higher than the estimation of data analyses of 1180 Mg yr^{-1} (Wang et al., 2016a). A part of the Hg from aboveground vegetation is released back into the atmosphere via photoreduction (234 Mg yr^{-1}) and wildfires (870 Mg yr^{-1}). Soil respiration also causes a re-emission of 982 Mg yr^{-1} to the atmosphere and an additional 216 Mg yr^{-1} and 122 Mg yr^{-1} are lost via leaching and runoff, respectively. The global soil Hg storage is estimated as 950 Gg (Fig. S3-S5), which is consistent with the range of 235–1150 Gg from previous studies (Amos et al., 2015, 2013; Selin et al., 2008; Wang et al., 2019). Due to the overall long residence time of soil Hg compared, we more focus on the vegetation part of the Hg cycle in this study.

3.2. Vegetation Hg(0) uptake

Fig. 2a shows the global distribution of vegetation uptake of Hg(0) based on the stomatal uptake scheme. Overall, field observations of Hg uptake by diverse vegetation are scarce. In general, the mean and standard error at the 39 observational sites are 42.93 ± 35 μg m^2 yr^{-1} for the model, consistent with the measurements (41.60 ± 46.80 μg m^2 yr^{-1}). Our stomatal uptake-based model also better captures the spatial patterns of observed vegetation Hg(0) uptake than the LAI scheme (Fig. 2b), especially in East Asia. The fitness between observation and model is also improved by our stomatal parameterization (Fig. 3a). Large variations are simulated across the biomes worldwide driven by vegetation (Fig. S6). A higher level of Hg(0) uptake by vegetation is modeled in the Amazon region (50.32 μg m^2 yr^{-1}) with the densest vegetation cover (Anadón et al., 2014) and higher net primary production (NPP) (Fig. S6) (Wang et al., 2021) despite the atmospheric Hg (0) concentrations over the Amazon area are relatively low (Fig. S1). This modeled Amazonian Hg(0) uptake by vegetation is comparable to the Hg deposition flux (averaged 49 μg m^2 yr^{-1}) by litterfall measurements (Fostier et al., 2015). Much lower Hg(0) uptake fluxes are simulated in areas lacking vegetation covers such as desert regions in Africa and Central Asia and the tundra area near the Arctic. Surprisingly, despite the lower NPP than the Amazon regions (Fig. S6b), we simulate the highest flux over East Asia (65 μg m^2 yr^{-1}) driven by the highest atmospheric Hg(0) concentrations (Figs. 2a, S1). This is consistent with in-situ observations (58.10 μg m^2 yr^{-1} in the central region of China by Yu et al. (2020) and 61 μg m^2 yr^{-1} in southwest of China by Luo et al. (2016)).

Fig. 2b shows the result if we adopt the LAI algorithm (Hg fixed by leaves through LAI) (Smith-Downey et al., 2010). The simulated Hg(0) uptake by the vegetation in the Amazon (51.73 μg m^2 yr^{-1}) is relatively higher than the East Asia (43.22 μg m^2 yr^{-1}).The vegetation uptake of Hg(0) over Amazon is likely to be overestimated by the LAI scheme. Since the LAI-based model does not consider the diurnal dynamics of leaves, such as the stomatal uptake process. Under low concentration conditions, the uptake of Hg by vegetation is less limited by stomatal uptake. This allows LAI similar to the stomatal uptake to estimate the uptake of atmospheric Hg(0) by foliar. However, at high mercury concentrations, the ability of vegetation to fix mercury leads to an underestimation of Hg (Fig. 3). The CLM5 considers the stomatal closure process occurring during the night or in situations like high water stress, which also hinders Hg(0) uptake by vegetation. Our model also suggests the East Asia as another region with significant difference between the LAI and stomatal approaches, mainly caused by the high atmospheric mercury concentrations in this region (Fig. S1a). The CLM5 includes a variety of vegetation types such as needle leaf species in this region, which have a relatively small leaf area but high update capacity of Hg (Luo et al., 2016). Our stomatal-based model indicates that this type of tree plays an important role in Hg(0) uptake with needleleaf evergreen tree (NET) accounting for 15% of total Hg assimilation (Fig. 4). In addition, the anthropogenic Hg emissions are the highest in East Asia (Zhang and Zhang, 2022), which amplifies the difference between the LAI and stomatal schemes in this region.

The global total Hg(0) flux assimilation by vegetation is modeled as 3138 Mg yr-^{1} (Fig. 1), which is higher than the LAI algorithm modeling 1788 Mg yr^{-1}. The total Hg assimilation by all PFTs is 2377 Mg yr^{-1}, with 290 Mg yr^{-1} for CFT (Fig. 4). The tropical/subtropical species accounts for the largest proportion (27.52%, 652 Mg yr^{-1}), followed by the temperate broadleaf deciduous (16%, 379 Mg yr^{-1}) and temperate needle-leaf evergreen (14.73%, 349 Mg yr^{-1}), consistent with previous studies (Wang et al., 2016a; Wohlgemuth et al., 2022; Zhou and Obrist, 2021). We find the foliar uptake of atmospheric Hg(0) is also regulated by tree functional traits, consistent with previous studies (Wohlgemuth et al., 2022). The CLM5 model divides vegetation into different phenological types based on temperature, soil moisture, day length, and the fraction of annual leaf growth. This approach helps to ensure that vegetation growth is more consistent with observations. In CLM5-Hg, evergreen vegetation types have the longest growing season, as their leaf growth cycle typically lasts for over a year or even longer (Wang et al., 2016b). Broadleaf tree species in CLM5 have a higher V_{cmax}, which reflects the photosynthetic rate of plant leaves. Indeed, tree species with larger leaf area can absorb more light photons (Teixeira et al., 2017), increasing A_n (the intensity of leaf net photosynthesis) and indirectly increasing stomatal conductance per unit of time for broadleaf species (via equation (3)), which we find facilities the uptake of more

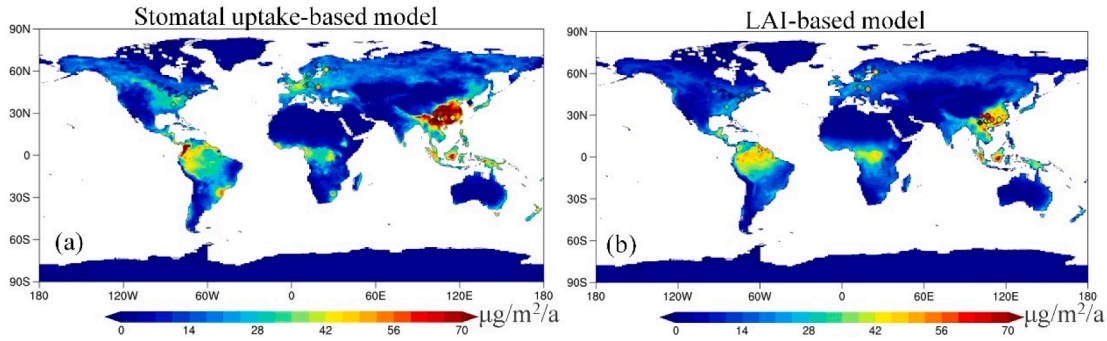

Fig. 2. Simulated global annual Hg(0) uptake by various plant functional type (PFT) uptake based on the parameterization of stomatal uptake (a) and the LAI algorithm (b). Model results (background) are the annual mean for the year 2014. Ground-based observations (rhombus) are obtained from the database of global vegetation measurements (See Methodology).

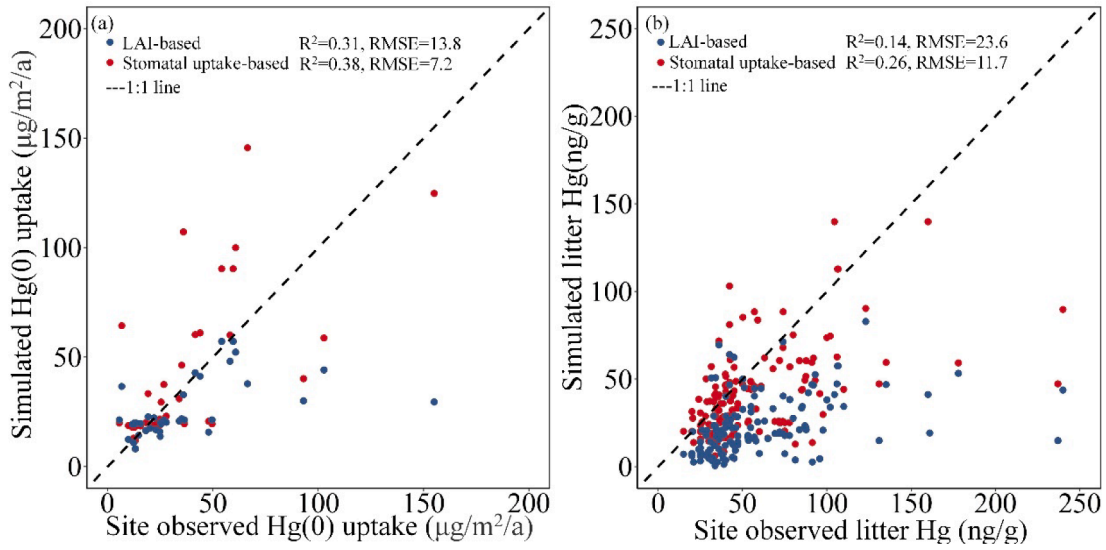

Fig. 3. Comparison between modeled and observed values for (a) Hg(0) uptake fluxes by vegetation and (b) litter Hg concentrations. Two sets of simulations are shown: LAI- and stomatal uptake-based.

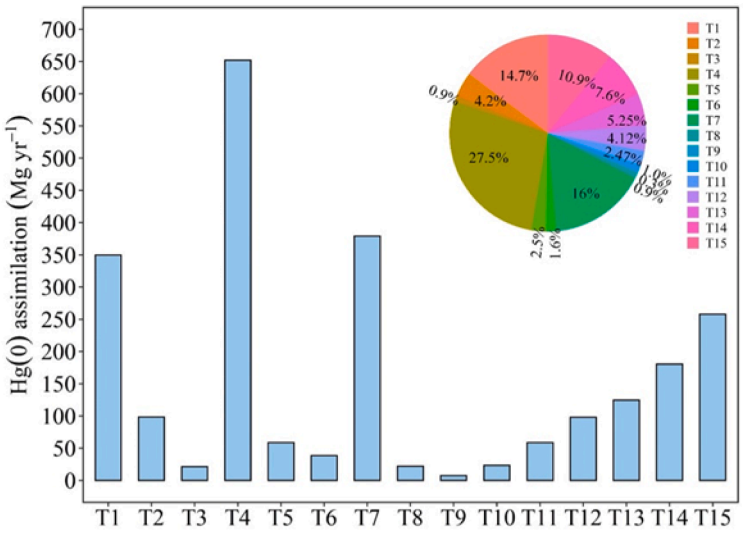

Fig. 4. Simulated global Hg assimilation by the vegetation of atmospheric Hg(0) separated via plant functional type (PFT). T1: Needleleaf evergreen tree (NET) – temperate, T2: Needleleaf evergreen tree – boreal, T3: Needleleaf deciduous tree (NDT) –boreal, T4: Broadleaf evergreen tree (BET) – tropical, T5: Broadleaf evergreen tree–temperate, T6: Broadleaf deciduous tree (BDT) –tropical, T7: Broadleaf deciduous tree–temperate, T8: Broadleaf deciduous tree–boreal, T9: Broadleaf evergreen shrub (BES) –temperate, T10: Broadleaf deciduous shrub (BDS) –temperate, T11: Broadleaf deciduous shrub– boreal, T12: C3 arctic grass, T13: C3 grass, T14: C4 grass, T15: Crops.

atmospheric Hg(0). As a result, our model suggests that tropical and subtropical tree species, represented by evergreen broadleaf forests, absorb the largest amount of Hg.

Our process-model-based estimate converges with the recent observation-derived estimate of global vegetation Hg assimilation flux scaled from direct Hg(0) measurements: 2113 ± 477 Mg yr^{-1} (Zhou and Obrist, 2021; Daniel et al., 2021). However, our estimate is much higher than Wang (Wang et al., 2016a) (1180 Mg yr^{-1}), which is based on litterfall data and may underestimate the vegetation Hg uptake. Moreover, their estimate does not the transformation time of mercury from leaves to litter, which is included in the phenology process in our model. Indeed, our model indicates that not all Hg(0) taken up by foliage is immediately senesced to litter on the surface soil. Our results are also higher than previous global atmospheric model estimates: e.g. 1180–1410 Mg yr^{-1} by Zhou et al. (2021), 730–1070 Mg yr^{-1} by Song et al. (2015), 1200 Mg yr^{-1} by Horowitz et al. (2017), and 2276 Mg yr^{-1} by Feinberg et al. (2022), because most of these models merely consider the land use types but not the specific PFT/CFT and the stomata uptake processes.

3.3. Litterfall Hg

Fig. 5a shows the global distribution of litterfall Hg concentrations, which is driven by that of Hg(0) uptake by vegetation (Fig. 2b) with high concentrations in regions like the Amazon and China and low concentrations in the desert and the Arctic. In general, our model captures the spatial patterns of observed litterfall Hg concentrations (Fig. 5a). The mean and standard deviation of litter Hg concentrations at the 187 sites are 46 ± 37 ng/g, close to the observations (59 ± 35 ng/g). Specifically, the model agrees well with the observations over eastern China, eastern North America, and West Europe, where the observations are the most adequate. The model also simulates relatively high litterfall Hg concentrations in southern Africa and Indonesia, where no observations exist yet. Moreover, compared with the result of the LAI-based approach, the fitness between observation and model is improved substantially by our stomatal parameterization (Fig. 3b). The model with stomatal parameterization also reduces the root mean square error (RMSE) between the model and observations by 50%. Our stomatal-based model considers the phenological process of vegetation from leaves to the formation of litter and includes the accumulation of

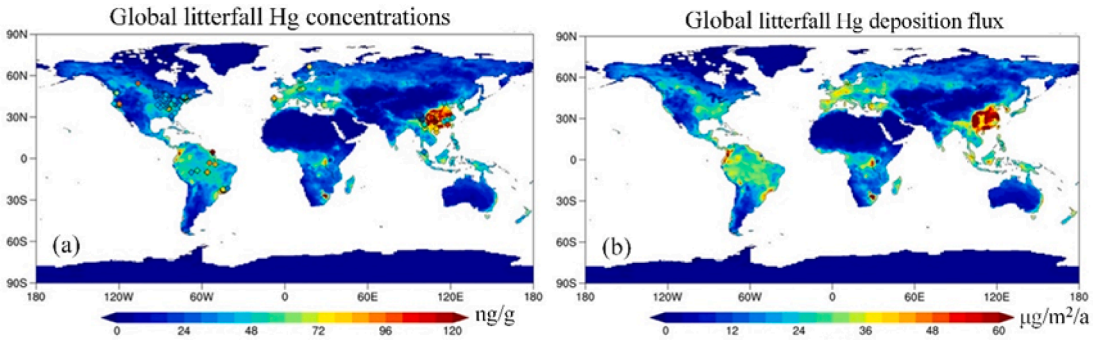

Fig. 5. Global distribution of litterfall Hg concentrations (a) and flux (b) simulated by CLM5-Hg. Model results (background) are the annual mean for the year 2014. Ground-based observations (rhombus) are obtained from the global Hg concentration of the plant tissue database (See Methodology).

mercury in leaves, which makes our model more in line with the actual growth of plants. On the contrary, the LAI algorithm is often implemented with satellite-derived monthly data without considering the detailed vegetation phenology (e.g., Smith-Downey et al., 2010).

Litterfall biomass is regarded as a key factor to determine the variation of atmospheric Hg input to the soil (Fig. S7) (Zhou et al., 2018), however, we find the atmospheric Hg(0) concentrations also play an important role (Fig. S1). Previous studies presumed that the highest litterfall Hg deposition occurred in the Amazon Region with the largest tree density and biomass production (Wang et al., 2016a). But in this study, the simulated litter Hg concentrations in the Amazon Region (63 ng/g) are lower than that in China (87 ng/g), which is likely attributed to higher litter Hg deposition in China (Fig. 5a and b). Indeed, the higher Hg(0) uptake by vegetation in East Asia results in more foliage Hg accumulation (Liu et al., 2021; Poissant, 2008). The relatively lower litterfall biomass in China (147 g m^2 yr^{-1}) also helps to concentrate the Hg in litter compared with the Amazon area (265 g m^2 yr^{-1}) (Fig. S7). Furthermore, for better nutrient management leading to an efficient resource economy for the production of new organs and plant fitness, nutrients (C, N) in leaf tissues can be translocated to other tissues before the leaf abscises in the CLM5 model (Lawrence et al., 2019), which decreases the mass density of the litterfall. However, as a non-nutrient element, such a recycling process is absent for Hg, which also amplifies the space–time asynchrony between litterfall Hg and biomass.

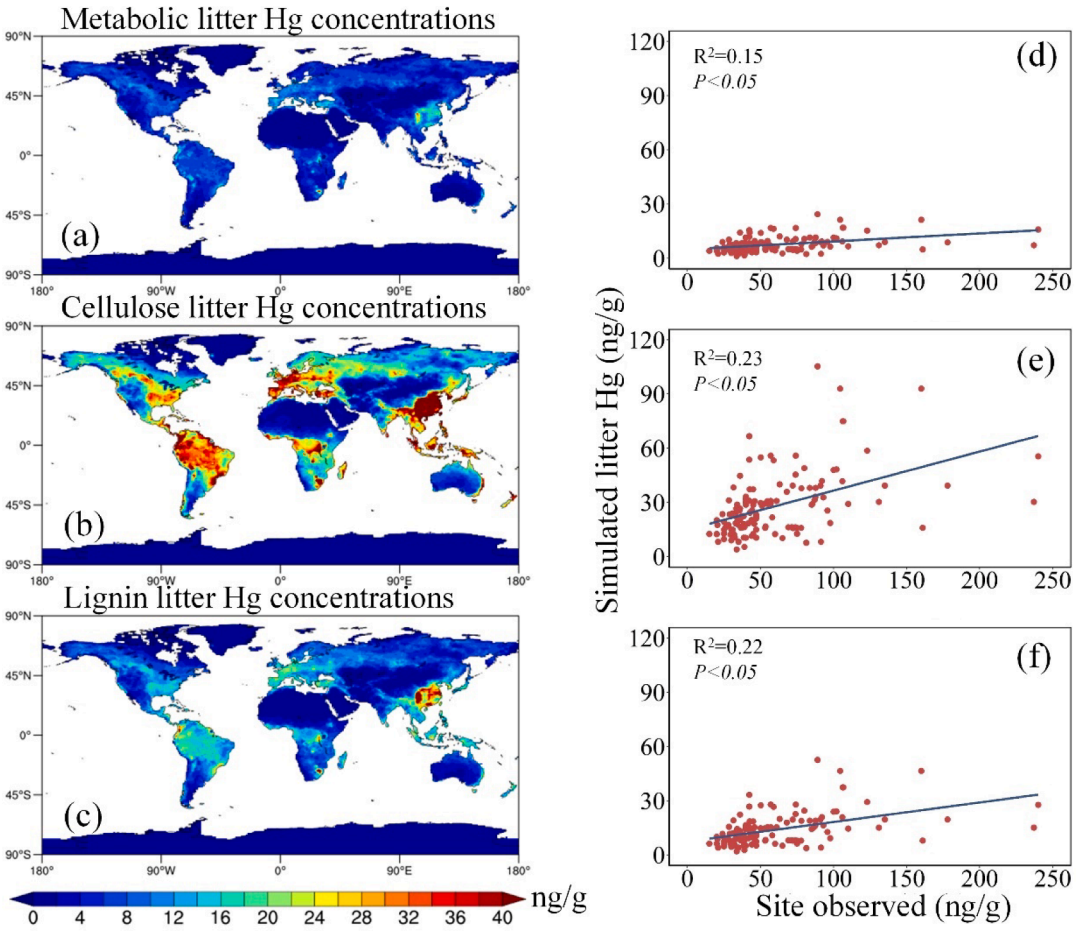

Fig. 6. Global distribution of simulated litterfall Hg concentration in aboveground pools: (a) metabolic litter (LITR1); (b) cellulose litter (LITR2); and (c) lignin litter (LITR3). Correlation of litter Hg concentration in observational sites and corresponding simulated value of aboveground pool from CLM5-Hg; (d) metabolic litter (LITR1) Hg versus Site observed litter Hg; (e) cellulose litter (LITR2) Hg versus Site observed litter Hg; (f) lignin litter (LITR3) Hg versus Site observed litter Hg.

The CLM5 model considers the metabolic litter pool, cellulose litter pool, and lignin litter pool, which have different decomposition rates and turnover times. Among them, the cellulose and lignin pools in the model have slower decomposition rates as they are polymerized carbohydrates and aromatic compounds that can resist microbial breakdown into smaller compounds for uptake (Kaiser et al., 2014; Mcclaugherty and Berg, 1987). The CLM5-Hg model simulates the spatial distribution of global Hg from these litter pools (Fig. 6a–c), generally consistent with the observations, including 331 individual data points across 139 different measurement sites spanning 21 years (1999–2020), which are extracted from a comprehensive database (Zhou et al., 2021). Our results show that the Hg deposition flux in cellulose (5.63 μg m^{-2} yr^{-1}) and lignin litter (2.82 μg m^{-2} yr^{-1}) is much higher than that in the metabolic litter (1.73 μg m^{-2} yr^{-1}). This indicates that the decomposition of litter mercury is strongly influenced by substrate quality, and the structural litter (cellulose litter + lignin litter) is a significant source of litter Hg (Fig. 6e and f). Moreover, the model also indicates that leaves with higher cellulose and lignin usually persist longer in the physiological processes, resulting in more accumulation of atmospheric Hg prior to forming litter.

3.4. Wildfire emissions

The global wildfire emissions of Hg are estimated as 870 Mg yr^{-1} (Fig. 1), which is equivalent to 22% of all currently known anthropogenic and natural mercury emissions (Shah et al., 2021). South America has the highest emissions, followed by the Middle East and Central America (Fig. 7). These regions usually have relatively longer dry periods, higher temperatures (>28℃), and intermediate annual rainfall (350–1100 nm) (Aldersley et al., 2011), which result in higher fire incidence. In contrast, South America and Africa of the Northern Hemisphere, as well as Arctic regions have less Hg emissions of wildfire (Fig. 7), potentially because of significant humid and wet conditions in tropical rainforest climate and less vegetation cover limiting burning area (Schuur, 2003). Our estimate is higher than previous studies (300–678 Mg yr^{-1}) (Friedli et al., 2009; Kumar et al., 2018; Sigler et al., 2003). One cause could be the larger Hg pools in the CLM5-Hg model which resulted from more vegetation uptake of Hg(0). Furthermore, our model considers more types of fire, such as deforestation fires and cropland fires. Our model also increases the mortality of vegetation induced by the fire with plant phenology (Lawrence et al., 2019).

3.5. Seasonal cycles

Fig. 8a–d shows the seasonal variation of Hg(0) vegetation uptake. The global Hg(0) vegetation uptake is 750 Mg yr^{-1} and 1050 Mg yr^{-1} during the period March-May (MAM) and the period June-August (JJA) respectively, which is higher than 350 Mg yr^{-1} and 250 Mg yr^{-1} during the period September-November (SON) and period December-February (DJF). Specifically, the highest uptake of Hg(0) by vegetation in the Northern Hemisphere occurs in JJA period, when East Asia, Europe, and temperate North America have 100 Mg yr^{-1}, 53 Mg yr^{-1}, and 65 Mg yr^{-1} vegetation Hg(0) uptake relatively, however, there is the largest vegetation uptake of Hg(0) in the Southern Hemisphere at DJF period, when 50 Mg yr^{-1} and 9 Mg yr^{-1} Hg(0) is uptake in South America and Southern Africa relatively. The seasonal variability of Hg(0) vegetation uptake is likely contributed by that of the plant growth, which is controlled by the dynamic parameters such as the temperature, precipitation, and solar radiation in the CLM5-Hg model. The rate of photosynthesis, which is determined by these parameters in the model, reaches its peak during the growing season of vegetation in the northern hemisphere. At this time, the stomatal conductance is also greater, allowing for more uptake of Hg(0) by vegetation in the spring and summer.

We find a lagging effect between Hg(0) vegetation uptake and litter Hg concentrations (Fig. 8e–h). It seems that simulated litter Hg concentrations are lagging for one season behind Hg(0) uptake. For BET-tropical forests, the water use efficiency (WUE) and soil water are higher during the growth season in our model, which promotes a large amount of litterfall deposition of Hg with the shedding of senescent leaves. Thus, a significant increase in litter Hg concentrations in China and the Amazon region begins in the JJA period (Fig. 8f), consistent with observed seasonal trends for the litter in the broad-leaved forest in southwest China (Zhou et al. 2018). However, our model suggests that deciduous trees such as BDT-temperate and BDT-boreal produce even more litterfall, which results in larger litterfall Hg deposition in temperate regions such as temperate North America, Europe, and Boreal Asia in the SON period (Fig. 8g). In the CLM5 model, any one of the following three conditions is sufficient to initiate the leaf-falling mechanism for deciduous phenology when autumn arrives: a sustained period of dry soil, a sustained period of cold temperature, or daylength shorter than six hours (Lawrence et al., 2019), and the leaf-falling during the SON period largely drives the strong Hg littering in these temperate regions. Although no observation data is available to evaluate our

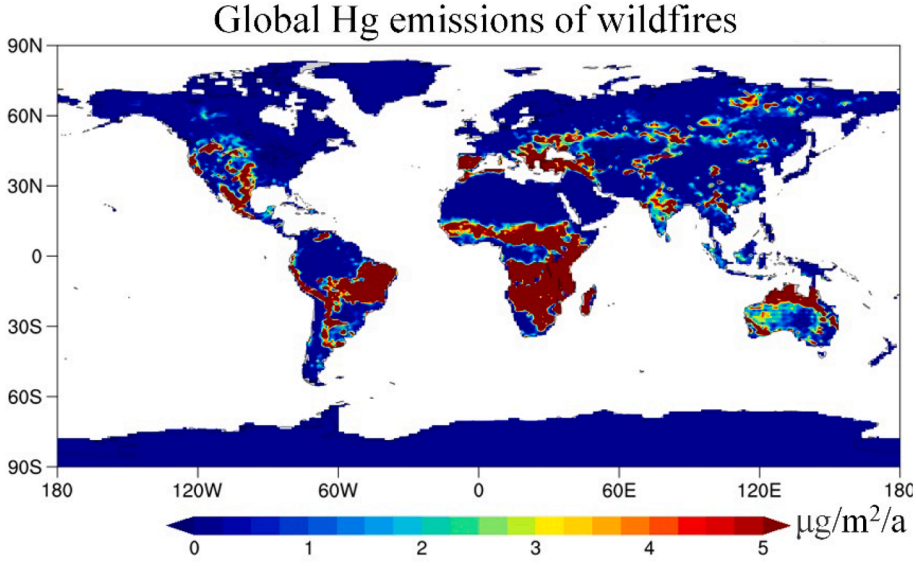

Fig. 7. Simulated Hg emissions of wildfires across the globe from CLM5-Hg.

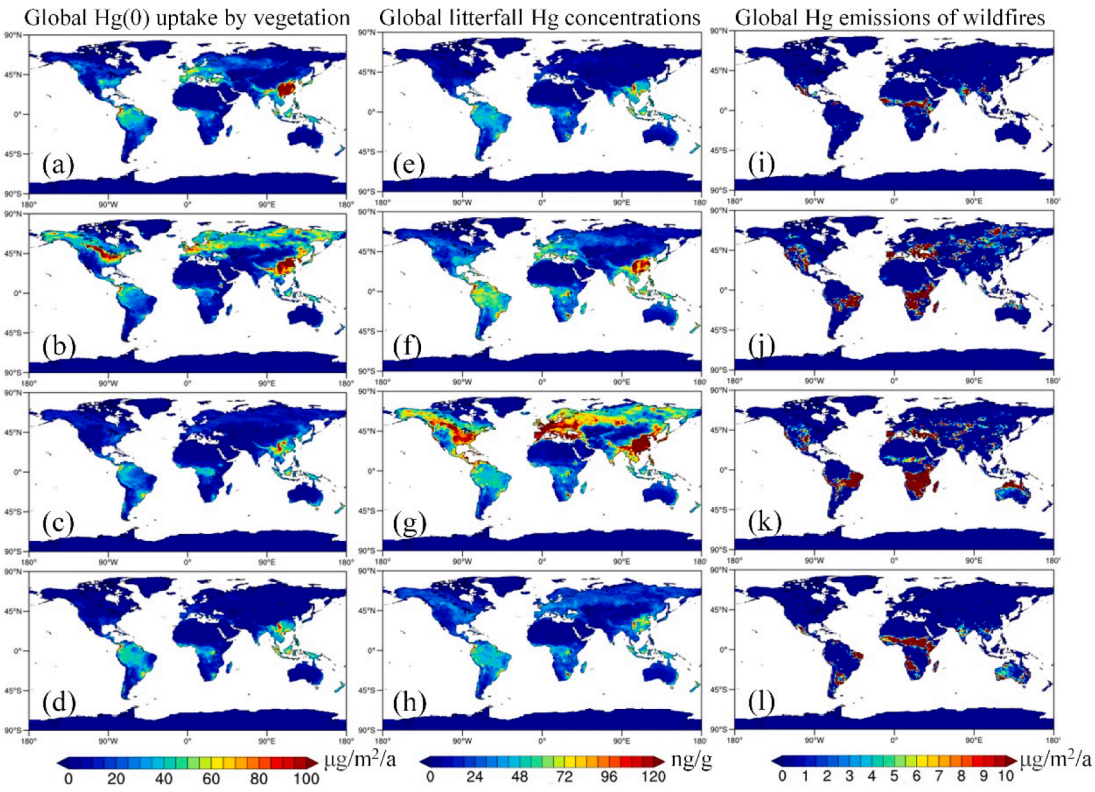

Fig. 8. The global seasonal pattern of Hg modeled by CLM5-Hg. (a.–d) Hg(0) uptake by vegetation; (e.–h) litterfall Hg concentration; (i.–l) Hg wildfire emissions. (a, e, i) MAM(March-May); (b, f, j) JJA(June-August); (c, g, k) SON(September-November); (d,h,l) DJF(December-February).

modeled results, yet, this implies that vegetation phenology is a potential influencing factor for the fate and mobility of Hg in forest floors, and the vegetation can buffer the air–soil exchange of Hg.

4. Uncertainties

The CLM5-Hg model bears substantial uncertainties. There is uncertainty for the modeled climatological forcing data such as temperature, relative humidity, precipitation, and short-wave radiation that impacts the plant physiology and soil C/N cycles (Fisher et al., 2019). The model parameterization and assumption of plant physiology such as photosynthesis, phenology, and evapotranspiration are also important sources of uncertainty (Lawrence et al., 2019). The representation of land cover/use is also limited by the model resolution (Chen et al., 2018; Meier et al., 2018). In addition, there are model structure uncertainties, such as the trade-off between the accuracy of vegetation biomass, leaf area, and soil moisture due to the difference in soil textures, depths, and seasons (Gao et al., 2021).

Our ability to model the speciation, transformation, transportation, and re-emission pattern of soil/vegetation Hg is limited by existing scientific knowledge and data. Many parameters in CLM5-Hg are not directly measured for Hg but analog to C, such as stomatal conductance, stabilization time of Hg in leaves, and the proportionality coefficient of Hg partitioning to various litter pools. There is also uncertainty about the association of these parameters with environmental factors and plant physiological characteristics as illustrated by Wang et al. (2016), Wohlgemuth et al. (2022), Zhou et al. (2021), whereas it is computationally prohibitive to evaluate these uncertainties quantitatively. We thus call for more mechanistic experimental studies in the future, to provide directly measured parameters related to Hg and the links with environment and plant physiology. Moreover, our model does not yet account for the transport and translocation of Hg between internal vegetation tissues, and neglects the root uptake of Hg from the soil, which may cause an underestimation of the vegetation Hg budget. In addition, we find various litter types contribute differently to the litter Hg flux but current measurement studies have covered very limited species. More data, especially for different plant species are needed to constrain the global litter Hg concentrations and fluxes.

5. Implications

We use so-far the most comprehensive global land model (CLM5-Hg) to simulate the land cycling of Hg at present-day. The model results indicate an annual vegetation uptake of Hg(0) of 3132 Mg yr^{-1}, which is considerably higher than previous global models and in line with most recent observational evidences. Considering a dynamic plant growth framework that includes stomatal uptake, CLM5-Hg can also simulate a more accurate global spatial distribution of Hg(0) deposition to land and litter Hg based on the current observational data and literature. Vegetation uptake of atmospheric Hg(0), together with litterfall biomass, are simulated as vital factors driving the global distribution of litter Hg, of which structural litter (cellulose litter + lignin litter) is a significant source. We identify a lagging effect between vegetation Hg(0) uptake and litter, representing a buffering effect for the exchange of Hg between the atmosphere and land. A similar buffering effect exists for the accumulation of vegetation Hg mass and wild fire emissions, which may also occur out of phase.

The buffering effect has a significant impact on the sequestration of anthropogenic Hg emissions by the global land. This effect thus needs to be considered in assessing the effectiveness of decreasing Hg use and emissions as prescribed in the Minamata Convention of Mercury (Selin et al., 2018). The simulated larger vegetation uptake in eastern China suggests the important role of atmospheric Hg concentrations, which helps to sequester the high anthropogenic emissions over this region, making a less global impact. This also indicates that the greenness of this region as a result of afforestation provides a potentially significant addition sink for atmospheric Hg (Wang et al., 2016b; Zhou et al., 2021). Our research calls for the protection of forests and the promotion of

afforestation, which plays a significant role for sequestering anthropogenic Hg emissions.

Terrestrial ecosystem processes, such as canopy gas exchanges, are sensitive to climate conditions and the responses differ among plant species. As the CLM5-Hg model links the terrestrial Hg cycle with plant physiology and the influencing climatological factors, it can diagnose the response of the terrestrial Hg cycle to the climate-driven changes in global vegetation. The model can also quantify the key processes of the terrestrial cycles of Hg, including litter decomposition and soil respiration. In addition, CLM5-Hg is now capable of considering various types of plants, expanding beyond the previous constraint of relying solely on satellite data for vegetation analysis. The use of prognostic phenology and active biogeochemistry can aid in predicting both short-term and long-term changes in Hg levels within vegetation and soil, enabling better monitoring of seasonal and environmental fluctuations. The effect of CO_2 fertilization and land use/land cover changes may have a large impact on vegetation uptake of Hg(0) by influencing stomatal resistance and dynamic vegetation structure (Zhang et al., 2016a; Zhao and Running, 2010). Furthermore, with increasing drought frequency and severity, the stomatal conductance will respond to changing environmental conditions (Anderegg et al., 2017), and the mortality of plants and wildfire events may alter the vegetation uptake and re-emissions of Hg under the scenarios of changing climate (Arora and Melton, 2018). Our model thus provides an ideal framework to predict the impact of future climate and global change on terrestrial Hg cycles, and helps understand the Hg dynamics across different spheres on the long-term trajectory of the Earth System.

CRediT authorship contribution statement

Tengfei Yuan: Conceptualization, Methodology, Formal analysis, Investigation, Data curation, Visualization, Writing – original draft. **Peng Zhang:** Methodology, Data curation, Validation, Resources. **Zhengcheng Song:** Investigation. **Shaojian Huang:** Investigation, Validation. **Xun Wang:** Resources, Validation. **Yanxu Zhang:** Conceptualization, Project administration, Validation, Data curation, Funding acquisition, Resources, Supervision, Writing – review & editing.

Declaration of Competing Interest

The authors declare that they have no known competing financial interests or personal relationships that could have appeared to influence the work reported in this paper.

Data availability

Data will be made available on request.

Acknowledgments

We acknowledge the financial support from the National Key R&D Program of China (2019YFA0606803), the Fundamental Research Funds for the Central Universities (14380168, 14380188), Frontiers Science Center for Critical Earth Material Cycling, and the Collaborative Innovation Center of Climate Change, Jiangsu Province.

Appendix A. Supplementary material

Supplementary data to this article can be found online at https://doi.org/10.1016/j.envint.2023.107904.

References

Agnan, Y., Le Dantec, T., Moore, C.W., Edwards, G.C., Obrist, D., 2016. New constraints on terrestrial surface-atmosphere fluxes of gaseous elemental mercury using a global database. Environ. Sci. Tech. 50 (2), 507–524. https://doi.org/10.1021/acs.est.5b04013.

Aldersley, A., Murray, S.J., Cornell, S.E., 2011. Global and regional analysis of climate and human drivers of wildfire. Sci. Total Environ. 409 (18), 3472–3481. https://doi.org/10.1016/j.scitotenv.2011.05.032.

Amos, H.M., Jacob, D.J., Streets, D.G., Sunderland, E.M., 2013. Legacy impacts of all-time anthropogenic emissions on the global mercury cycle. Global Biogeochem. Cycles 27 (2), 410–421. https://doi.org/10.1002/gbc.20040.

Amos, H.M., Sonke, J.E., Obrist, D., Robins, N., Hagan, N., Horowitz, H.M., Mason, R.P., Witt, M., Hedgecock, I.M., Corbitt, E.S., Sunderland, E.M., 2015. Observational and modeling constraints on global anthropogenic enrichment of mercury. Environ. Sci. Tech. 49 (7), 4036–4047. https://doi.org/10.1021/es5058665.

Anadón, J.D., Sala, O.E., Maestre, F.T., 2014. Climate change will increase savannas at the expense of forests and treeless vegetation in tropical and subtropical Americas. J. Ecol. 102 (6), 1363–1373. https://doi.org/10.1111/1365-2745.12325.

Anderegg, W.R.L., Wolf, A., Arango-Velez, A., Choat, B., Chmura, D.J., Jansen, S., Kolb, T., Li, S., Meinzer, F., Pita, P., de Dios, V.R., Sperry, J.S., Wolfe, B.T., Pacala, S., 2017. Plant water potential improves prediction of empirical stomatal models. PLoS One 12 (10), e0185481.

Arora, V.K., Melton, J.R., 2018. Reduction in global area burned and wildfire emissions since 1930s enhances carbon uptake by land. Nat. Commun. 9 (1), 1326-. https://doi.org/10.1038/s41467-018-03838-0.

Bash, J.O., 2010. Description and initial simulation of a dynamic bidirectional air-surface exchange model for mercury in Community Multiscale Air Quality (CMAQ) model. J. Geophys. Res. Atmos. 115 (6), 1–15. https://doi.org/10.1029/2009JD012834.

Beckers, F., Rinklebe, J., 2017. Cycling of mercury in the environment: sources, fate, and human health implications: a review. Crit. Rev. Environ. Sci. Technol. 47 (9), 693–794. https://doi.org/10.1080/10643389.2017.1326277.

Chen, L., Dirmeyer, P.A., Guo, Z., Schultz, N.M., 2018. Pairing fluxnet sites to validate model representations of land-use/land-cover change. Hydrol. Earth Syst. Sci. 22 (1), 111–125. https://doi.org/10.5194/hess-22-111-2018.

Daniel, O., M., R.E., L., H.J., F., K.C., William, M.J., Hans, M., D., R.C., Shiwei, S., Jun, Z., Róisín, C., 2021. Previously unaccounted atmospheric mercury deposition in a midlatitude deciduous forest. Proc. Nat. Acad. Sci. 118 (29), e2105477118 doi: 10.1073/pnas.2105477118.

De Kauwe, M.G., Kala, J., Lin, Y.-S., Pitman, A.J., Medlyn, B.E., Duursma, R.A., Abramowitz, G., Wang, Y.-P., Miralles, D.G., 2015. A test of an optimal stomatal conductance scheme within the CABLE land surface model. Geosci. Model Dev. 8 (2), 431–452. https://doi.org/10.5194/gmd-8-431-2015.

De Simone, F., Cinnirella, S., Gencarelli, C.N., Yang, X., Hedgecock, I.M., Pirrone, N., 2015. Model study of global mercury deposition from biomass burning. Environ. Sci. Tech. 49 (11), 6712–6721. https://doi.org/10.1021/acs.est.5b00969.

Fay, L., Gustin, M., 2007. Assessing the influence of different atmospheric and soil mercury concentrations on foliar mercury concentrations in a controlled environment. Water Air Soil Pollut. 181 (1), 373–384. https://doi.org/10.1007/s11270-006-9308-6.

Feinberg, A., Dlamini, T., Jiskra, M., Shah, V., Selin, N.E., 2022. Evaluating atmospheric mercury (Hg) uptake by vegetation in a chemistry-transport model. Environ. Sci. Processes Impacts 24 (9), 1303–1318. https://doi.org/10.1039/D2EM00032F.

Fisher, R.A., Wieder, W.R., Sanderson, B.M., Koven, C.D., Oleson, K.W., Xu, C., Fisher, J. B., Shi, M., Walker, A.P., Lawrence, D.M., 2019a. Parametric controls on vegetation responses to biogeochemical forcing in the CLM5. J. Adv. Model. Earth Syst. 11, 2879–2895. https://doi.org/10.1029/2019MS001609.

Fostier, A.H., Melendez-Perez, J.J., Richter, L., 2015. Litter mercury deposition in the Amazonian rainforest. Environ. Pollut. 206, 605–610. https://doi.org/10.1016/j.envpol.2015.08.010.

Fisher, R.A., Wieder, W.R., Sanderson, B.M., Koven, C.D., Oleson, K.W., Xu, C., Fisher, J. B., Shi, M., Walker, A.P., Lawrence, D.M., 2019b. Parametric controls on vegetation responses to biogeochemical forcing in the CLM5. J. Adv. Model. Earth Syst. 11 (9), 2879–2895. https://doi.org/10.1029/2019MS001609.

Friedli, H.R., Arellano, A.F., Cinnirella, S., Pirrone, N., 2009. Initial estimates of mercury emissions to the atmosphere from global biomass burning. Environ. Sci. Tech. 43 (10), 3507–3513. https://doi.org/10.1021/es802703g.

Fu, X., Zhang, H., Liu, C., Zhang, H., Lin, C.-J., Feng, X., 2019. Significant seasonal variations in isotopic composition of atmospheric total gaseous mercury at forest sites in china caused by vegetation and mercury sources. Environ. Sci. Tech. 53 (23), 13748–13756. https://doi.org/10.1021/acs.est.9b05016.

Gao, X., Avramov, A., Saikawa, E., Schlosser, C.A., 2021. Emulation of Community Land Model Version 5 (CLM5) to quantify sensitivity of soil moisture to uncertain parameters. J. Hydrometeorol. 22 (2), 259–278. https://doi.org/10.1175/JHM-D-20-0043.1.

Gustin, M.S., Lindberg, S.E., Weisberg, P.J., 2008. An update on the natural sources and sinks of atmospheric mercury. Appl. Geochem. 23 (3), 482–493. https://doi.org/10.1016/j.apgeochem.2007.12.010.

Gworek, B., Dmuchowski, W., Baczewska-Dąbrowska, A.H., 2020. Mercury in the terrestrial environment: a review. Environ. Sci. Eur. 32, 128. https://doi.org/10.1186/s12302-020-00401-x.

Horowitz, H.M., Jacob, D.J., Zhang, Y., Dibble, T.S., Slemr, F., Amos, H.M., Schmidt, J. A., Corbitt, E.S., Marais, E.A., Sunderland, E.M., 2017. A new mechanism for atmospheric mercury redox chemistry: implications for the global mercury budget. Atmos. Chem. Phys. 17 (10), 6353–6371. https://doi.org/10.5194/acp-17-6353-2017.

Jiskra, M., Sonke, J.E., Obrist, D., Bieser, J., Ebinghaus, R., Myhre, C.L., Pfaffhuber, K.A., Wängberg, I., Kyllönen, K., Worthy, D., Martin, L.G., Labuschagne, C., Mkololo, T., Ramonet, M., Magand, O., Dommergue, A., 2018. A vegetation control on seasonal variations in global atmospheric mercury concentrations. Nat. Geosci. 11 (4), 244–250. https://doi.org/10.1038/s41561-018-0078-8.

Jiskra, M., Wiederhold, J.G., Skyllberg, U., Kronberg, R.-M., Hajdas, I., Kretzschmar, R., 2015. Mercury deposition and re-emission pathways in boreal forest soils investigated with Hg Isotope signatures. Environ. Sci. Tech. 49 (12), 7188–7196. https://doi.org/10.1021/acs.est.5b00742.

Kaiser, C., Franklin, O., Dieckmann, U., Richter, A., 2014. Microbial community dynamics alleviate stoichiometric constraints during litter decay. Ecol. Lett. 17 (6), 680–690. https://doi.org/10.1111/ele.12269.

Khan, T.R., Obrist, D., Agnan, Y., Selin, N.E., Perlinger, J.A., 2019. Atmosphere-terrestrial exchange of gaseous elemental mercury: parameterization improvement through direct comparison with measured ecosystem fluxes. Environ. Sci. Process. Impacts 21 (10), 1699–1712. https://doi.org/10.1039/C9EM00341J.

Kohlenberg, A.J., Turetsky, M.R., Thompson, D.K., Branfireun, B.A., Mitchell, C.P.J., 2018. Controls on boreal peat combustion and resulting emissions of carbon and mercury. Environ. Res. Lett. 13 (3), 35005. https://doi.org/10.1088/1748-9326/aa9ea8.

Kumar, A., Wu, S., Huang, Y., Liao, H., Kaplan, J.O., 2018. Mercury from wildfires: global emission inventories and sensitivity to 2000–2050 global change. Atmos. Environ. 173, 6–15. https://doi.org/10.1016/j.atmosenv.2017.10.061.

Laacouri, A., Nater, E.A., Kolka, R.K., 2013. Distribution and uptake dynamics of mercury in leaves of common deciduous tree species in minnesota, U.S.A. Environ. Sci. Tech. 47 (18), 10462–10470. https://doi.org/10.1021/es401357z.

Lawrence, D.M., Fisher, R.A., Koven, C.D., Oleson, K.W., Swenson, S.C., Bonan, G., Collier, N., Ghimire, B., van Kampenhout, L., Kennedy, D., Kluzek, E., Lawrence, P.J., Li, F., Li, H., Lombardozzi, D., Riley, W.J., Sacks, W.J., Shi, M., Vertenstein, M., Wieder, W.R., Xu, C., Ali, A.A., Badger, A.M., Bisht, G., van den Broeke, M., Brunke, M.A., Burns, S.P., Buzan, J., Clark, M., Craig, A., Dahlin, K., Drewniak, B., Fisher, J.B., Flanner, M., Fox, A.M., Gentine, P., Hoffman, F., Keppel-Aleks, G., Knox, R., Kumar, S., Lenaerts, J., Leung, L.R., Lipscomb, W.H., Lu, Y., Pandey, A., Pelletier, J.D., Perket, J., Randerson, J.T., Ricciuto, D.M., Sanderson, B.M., Slater, A., Subin, Z.M., Tang, J., Thomas, R.Q., Val Martin, M., Zeng, X., 2019. The community land model version 5: description of new features, benchmarking, and impact of forcing uncertainty. J. Adv. Model. Earth Syst. 11 (12), 4245–4287. https://doi.org/10.1029/2018MS001583.

Lawrence, D.M., Hurtt, G.C., Arneth, A., Brovkin, V., Calvin, K.V., Jones, A.D., Jones, C. D., Lawrence, P.J., de Noblet-Ducoudré, N., Pongratz, J., Seneviratne, S.I., Shevliakova, E., 2016. The Land Use Model Intercomparison Project (LUMIP) contribution to CMIP6: rationale and experimental design. Geosci. Model Dev. 9 (9), 2973–2998. https://doi.org/10.5194/gmd-9-2973-2016.

Li, S., Yuan, W., Ciais, P., Viovy, N., Ito, A., Jia, B., Zhu, D., 2019. Benchmark estimates for aboveground litterfall data derived from ecosystem models. Environ. Res. Lett. 14 (8), 84020. https://doi.org/10.1088/1748-9326/ab2ee4.

Liu, Y., Liu, G., Wang, Z., Guo, Y., Yin, Y., Zhang, X., Cai, Y., Jiang, G., 2021. Understanding foliar accumulation of atmospheric Hg in terrestrial vegetation: progress and challenges. Crit. Rev. Environ. Sci. Technol. 52 (24), 4331–4352. https://doi.org/10.1080/10643389.2021.1989235.

Luo, K., Yuan, W., Liu, N., Zeng, S., Wang, D., Lu, Z., Wang, X., Feng, X., 2022. Remarkable variation in the process of hg accumulation in timberline forests indicates an aggravated hg burden in alpine forests under climate warming. journal of geophysical research. Biogeosciences 127 (9). https://doi.org/10.1029/2022JG006940 e2022JG006940.

Luo, Y., Duan, L., Driscoll, C.T., Xu, G., Shao, M., Taylor, M., Wang, S., Hao, J., 2016. Foliage/atmosphere exchange of mercury in a subtropical coniferous forest in south China. J. Geophys. Res. Biogeo. 121 (7), 2006–2016. https://doi.org/10.1002/2016JG003388.

Mcclaugherty, C., Berg, B., 1987. Cellulose, lignin and nitrogen concentrations as rate regulating factors in late stages of forest litter decomposition. Pedobiologia 30, 101–112.

Medlyn, B.E., Duursma, R.A., Eamus, D., Ellsworth, D.S., Colin Prentice, I., Barton, C.V. M., Crous, K.Y., de Angelis, P., Freeman, M., Wingate, L., 2012. Reconciling the optimal and empirical approaches to modelling stomatal conductance. Glob. Chang. Biol. 18 (11), 3476. https://doi.org/10.1111/j.1365-2486.2012.02790.x.

Meier, R., Davin, E.L., Lejeune, Q., Hauser, M., Li, Y., Martens, B., Schultz, N.M., Sterling, S., Thiery, W., 2018. Evaluating and improving the Community Land Model's sensitivity to land cover. Biogeosciences 15, 4731–4757. https://doi.org/10.5194/bg-15-4731-2018.

Millhollen, A.G., Gustin, M.S., Obrist, D., 2006. Foliar mercury accumulation and exchange for three tree species. Environ. Sci. Tech. 40 (19), 6001–6006. https://doi.org/10.1021/es0609194.

Miretzky, P., Bisinoti, M.C., Jardim, W.F., 2005. Sorption of mercury (II) in Amazon soils from column studies. Chemosphere 60 (11), 1583–1589. https://doi.org/10.1016/j.chemosphere.2005.02.050.

Obrist, D., Agnan, Y., Jiskra, M., Olson, C.L., Colegrove, D.P., Hueber, J., Moore, C.W., Sonke, J.E., Helmig, D., 2017. Tundra uptake of atmospheric elemental mercury drives Arctic mercury pollution. Nature 547 (7662), 201–204. https://doi.org/10.1038/nature22997.

Obrist, D., Kirk, J.L., Zhang, L., Sunderland, E.M., Jiskra, M., Selin, N.E., 2018. A review of global environmental mercury processes in response to human and natural perturbations: changes of emissions, climate, and land use. Ambio 47 (2), 116–140. https://doi.org/10.1007/s13280-017-1004-9.

Outridge, P.M., Mason, R.P., Wang, F., Guerrero, S., Heimbürger-Boavida, L.E., 2018. Updated global and oceanic mercury budgets for the united nations global mercury assessment 2018. Environ. Sci. Tech. 52 (20), 11466–11477. https://doi.org/10.1021/acs.est.8b01246.

Poissant, 2008. Mercury concentrations and foliage_atmosphere fluxes in a maple forest ecosystem in Québec. Canada. J. Geophys. Res. 8 (9), 2507–2521.

Pokharel, A.K., Obrist, D., 2011. Fate of mercury in tree litter during decomposition. Biogeosciences 8 (9), 2507–2521. https://doi.org/10.5194/bg-8-2507-2011.

Risch, M.R., DeWild, J.F., Krabbenhoft, D.P., Kolka, R.K., Zhang, L., 2012. Litterfall mercury dry deposition in the eastern USA. Environ. Pollut. 161, 284–290. https://doi.org/10.1016/j.envpol.2011.06.005.

Rutter, A.P., Schauer, J.J., Shafer, M.M., Creswell, J., Olson, M.R., Clary, A., Robinson, M., Parman, A.M., Katzman, T.L., 2011a. Climate sensitivity of gaseous elemental mercury dry deposition to plants: impacts of temperature, light intensity, and plant species. Environ. Sci. Tech. 45 (2), 569–575. https://doi.org/10.1021/es102687b.

Rutter, A.P., Schauer, J.J., Shafer, M.M., Creswell, J.E., Olson, M.R., Robinson, M., Collins, R.M., Parman, A.M., Katzman, T.L., Mallek, J.L., 2011b. Dry deposition of gaseous elemental mercury to plants and soils using mercury stable isotopes in a controlled environment. Atmos. Environ. 45, 848–855. https://doi.org/10.1016/j.atmosenv.2010.11.025.

Saiz-Lopez, A., Sitkiewicz, S.P., Roca-Sanjuán, D., Oliva-Enrich, J.M., Dávalos, J.Z., Notario, R., Jiskra, M., Xu, Y., Wang, F., Thackray, C.P., Sunderland, E.M., Jacob, D. J., Travnikov, O., Cuevas, C.A., Acuña, A.U., Rivero, D., Plane, J.M.C., Kinnison, D. E., Sonke, J.E., 2022. Author Correction: Photoreduction of gaseous oxidized mercury changes global atmospheric mercury speciation, transport and deposition. Nat. Commun. 13 (1), 881. https://doi.org/10.1038/s41467-022-28455-w.

Schaefer, K., Elshorbany, Y., Jafarov, E., Schuster, P.F., Striegl, R.G., Wickland, K.P., Sunderland, E.M., 2020. Potential impacts of mercury released from thawing permafrost. Nat. Commun. 11 (1), 4650. https://doi.org/10.1038/s41467-020-18398-5.

Schuur, E.A.G., 2003. Productivity and global climate revisited: the sensitivity of tropical forest growth to precipitation. Ecology 84 (5), 1165–1170. https://doi.org/10.1890/0012-9658(2003)084[1165:PAGCRT]2.0.CO;2.

Selin, N.E., Jacob, D.J., Yantosca, R.M., Strode, S., Jaeglé, L., Sunderland, E.M., 2008. Global 3-D land-ocean-atmosphere model for mercury: present-day versus preindustrial cycles and anthropogenic enrichment factors for deposition. Global Biogeochem. Cycles 22, GB2011. https://doi.org/10.1029/2007GB003040.

Selin, H., Keane, S.E., Wang, S., Selin, N.E., Davis, K., Ambio, D.E., 2018. Linking science and policy to support the implementation of the Minamata Convention on Mercury. Ambio 47, 198–215. https://doi.org/10.1007/s13280-017-1003-x.

Shah, V., Jacob, D.J., Thackray, C.P., Wang, X., Sunderland, E.M., Dibble, T.S., Saiz-Lopez, A., Černušák, I., Kellö, V., Castro, P.J., Wu, R., Wang, C., 2021. Improved mechanistic model of the atmospheric redox chemistry of mercury. Environ. Sci. Tech. 55 (21), 14445–14456. https://doi.org/10.1021/acs.est.1c03160.

Sigler, J.M., Lee, X., Munger, W., 2003. Emission and long-range transport of gaseous mercury from a large-scale canadian boreal forest fire. Environ. Sci. Tech. 37 (19), 4343–4347. https://doi.org/10.1021/es026401r.

Smith-Downey, N.V., Sunderland, E.M., Jacob, D.J., 2010. Anthropogenic impacts on global storage and emissions of mercury from terrestrial soils: insights from a new global model. J. Geophys. Res. Biogeosci. 115 (G3) https://doi.org/10.1029/2009JG001124.

Song, S., Selin, N.E., Soerensen, A.L., Angot, H., Artz, R., Brooks, S., Brunke, E.-G., Conley, G., Dommergue, A., Ebinghaus, R., Holsen, T.M., Jaffe, D.A., Kang, S., Kelley, P., Luke, W.T., Magand, O., Marumoto, K., Pfaffhuber, K.A., Ren, X., Sheu, G.-R., Slemr, F., Warneke, T., Weigelt, A., Weiss-Penzias, P., Wip, D.C., Zhang, Q., 2015. Top-down constraints on atmospheric mercury emissions and implications for global biogeochemical cycling. Atmos. Chem. Phys. 15 (12), 7103–7125. https://doi.org/10.5194/acp-15-7103-2015.

St. Louis, V.L., Graydon, J.A., Lehnherr, I., Amos, H.M., Sunderland, E.M., St. Pierre, K. A., Emmerton, C.A., Sandilands, K., Tate, M., Steffen, A., Humphreys, E.R., 2019. Atmospheric concentrations and wet/dry loadings of mercury at the remote experimental lakes area, Northwestern Ontario, Canada. Environ. Sci. Tech. 53 (14), 8017–8026.

Stamenkovic, J., Gustin, M.S., 2009. Nonstomatal versus stomatal uptake of atmospheric mercury. Environ. Sci. Tech. 43 (5), 1367–1372. https://doi.org/10.1021/es801583a.

Sun, T., Ma, M., Wang, X., Wang, Y., Du, H., Xiang, Y., Xu, Q., Xie, Q., Wang, D., 2019. Mercury transport, transformation and mass balance on a perspective of hydrological processes in a subtropical forest of China. Environ. Pollut. 254, 113065 https://doi.org/10.1016/j.envpol.2019.113065.

Teixeira, D.C., Lacerda, L.D., Silva-Filho, E.V., 2017. Mercury sequestration by rainforests: the influence of microclimate and different successional stages. Chemosphere 168, 1186–1193. https://doi.org/10.1016/j.chemosphere.2016.10.081.

Wang, X., Bao, Z., Lin, C.-J., Yuan, W., Feng, X., 2016a. Assessment of global mercury deposition through litterfall. Environ. Sci. Tech. 50 (16), 8548–8557. https://doi.org/10.1021/acs.est.5b06351.

Wang, X., Lin, C.-J., Lu, Z., Zhang, H., Zhang, Y., Feng, X., 2016b. Enhanced accumulation and storage of mercury on subtropical evergreen forest floor: implications on mercury budget in global forest ecosystems. J. Geophys. Res. Biogeo. 121 (8), 2096–2109. https://doi.org/10.1002/2016JG003446.

Wang, X., Lin, C.-J., Yuan, W., Sommar, J., Zhu, W., Feng, X., 2016c. Emission-dominated gas exchange of elemental mercury vapor over natural surfaces in China. Atmos. Chem. Phys. 16, 11125–11143. https://doi.org/10.5194/acp-16-11125-2016.

Wang, X., Lin, C.-J., Yuan, W., Sommar, J., Zhu, W., Feng, X., 2016d. Emission-dominated gas exchange of elemental mercury vapor over natural surfaces in China. Atmos. Chem. Phys. 16 (17), 11125–11143. https://doi.org/10.5194/acp-16-11125-2016.

Wang, X., Luo, J., Yin, R., Yuan, W., Lin, C.-J., Sommar, J., Feng, X., Wang, H., Lin, C., 2017. Using mercury isotopes to understand mercury accumulation in the montane

forest floor of the Eastern Tibetan plateau. Environ. Sci. Tech. 51 (2), 801–809. https://doi.org/10.1021/acs.est.6b03806.

Wang, X., Yuan, W., Lin, C.-J., Feng, X., 2021. Mercury cycling and isotopic fractionation in global forests. Crit. Rev. Environ. Sci. Technol. 52 (21), 3763–3786. https://doi.org/10.1080/10643389.2021.1961505.

Wang, X., Yuan, W., Lin, C.-J., Zhang, L., Zhang, H., Feng, X., 2019. Climate and vegetation as primary drivers for global mercury storage in surface soil. Environ. Sci. Tech. 53 (18), 10665–10675. https://doi.org/10.1021/acs.est.9b02386.

Wesely, M.L., 1989. Parameterization of surface resistances to gaseous dry deposition in regional-scale numerical models. Atmos. Environ. 23 (6), 1293 doi:10.1016/0004-6981(89)90153-4.

Wohlgemuth, L., Rautio, P., Ahrends, B., Russ, A., Vesterdal, L., Waldner, P., Timmermann, V., Eickenscheidt, N., Fürst, A., Greve, M., Roskams, P., Thimonier, A., Nicolas, M., Kowalska, A., Ingerslev, M., Merilä, P., Benham, S., Iacoban, C., Hoch, G., Alewell, C., Jiskra, M., 2022. Physiological and climate controls on foliar mercury uptake by European tree species. Biogeosciences 19 (5), 1335–1353. https://doi.org/10.5194/bg-19-1335-2022.

Yu, Q., Luo, Y., Xu, G., Wu, Q., Wang, S., Hao, J., Duan, L., 2020. Subtropical forests act as mercury sinks but as net sources of gaseous elemental mercury in South China. Environ. Sci. Tech. 54 (5), 2772–2779. https://doi.org/10.1021/acs.est.9b06715.

Yuan, W., Sommar, J., Lin, C.-J., Wang, X., Li, K., Liu, Y., Zhang, H., Lu, Z., Wu, C., Feng, X., 2019a. Stable isotope evidence shows re-emission of elemental mercury vapor occurring after reductive loss from foliage. Environ. Sci. Tech. 53 (2), 651–660. https://doi.org/10.1021/acs.est.8b04865.

Yuan, W., Wang, X., Lin, C.-J., Sommar, J., Lu, Z., Feng, X., 2019b. Process factors driving dynamic exchange of elemental mercury vapor over soil in broadleaf forest ecosystems. Atmos. Environ. 219, 117047 https://doi.org/10.1016/j.atmosenv.2019.117047.

Zhang, H., Holmes, C.D., Wu, S., 2016a. Impacts of changes in climate, land use and land cover on atmospheric mercury. Atmos. Environ. 141, 230–244. https://doi.org/10.1016/j.atmosenv.2016.06.056.

Zhang, L., Wu, Z., Cheng, I., Paige Wright, L., Olson, M.L., Gay, D.A., Risch, M.R., Brooks, S., Castro, M.S., Conley, G.D., Edgerton, E.S., Holsen, T.M., Luke, W., Tordon, R., Weiss-Penzias, P., 2016b. The estimated six-year mercury dry deposition across North America. Environ. Sci. Tech. 50 (23), 12864–12873. https://doi.org/10.1021/acs.est.6b04276.

Zhang, P., Zhang, Y., 2022. Earth system modeling of mercury using CESM2 – Part 1: Atmospheric model CAM6-Chem/Hg v1.0. Geosci. Model Dev. 15 (9), 3587–3601. https://doi.org/10.5194/gmd-15-3587-2022.

Zhang, Z.-Y., Li, G., Yang, L., Wang, X.-J., Sun, G.-X., 2020. Mercury distribution in the surface soil of China is potentially driven by precipitation, vegetation cover and organic matter. Environ. Sci. Eur. 32 (1), 89. https://doi.org/10.1186/s12302-020-00370-1.

Zhao, M., Running, S.W., 2010. Drought-induced reduction in global terrestrial net primary production from 2000 through 2009. Science 329 (5994), 940–943. https://doi.org/10.1126/science.1192666.

Zhou, J., Obrist, D., 2021. Global mercury assimilation by vegetation. Environ. Sci. Tech. 55 (20), 14245–14257. https://doi.org/10.1021/acs.est.1c03530.

Zhou, J., Obrist, D., Dastoor, A., Jiskra, M., Ryjkov, A., 2021. Vegetation uptake of mercury and impacts on global cycling. Nat. Rev. Earth Environ. 2 (4), 269–284. https://doi.org/10.1038/s43017-021-00146-y.

Zhou, J., Wang, Z., Sun, T., Zhang, H., Zhang, X., 2016. Mercury in terrestrial forested systems with highly elevated mercury deposition in southwestern China: the risk to insects and potential release from wildfires. Environ. Pollut. 212, 188–196. https://doi.org/10.1016/j.envpol.2016.01.003.

Zhou, J., Wang, Z., Zhang, X., 2018. Deposition and fate of mercury in litterfall, litter, and soil in coniferous and broad-leaved forests. J. Geophys. Res. Biogeo. 123 (8), 2590–2603. https://doi.org/10.1029/2018JG004415.